ACS APPLIED MATERIALS & INTERFACES

Research Article

www.acsami.org

Solution-Blown Core–Shell Self-Healing Nano- and Microfibers

Min Wook Lee,[†] Sam S. Yoon,[*,‡] and Alexander L. Yarin[*,†,‡]

[†]Department of Mechanical and Industrial Engineering, University of Illinois, Chicago, Illinois 60607-7022, United States

[‡]School of Mechanical Engineering, Korea University, Seoul 136-713, Republic of Korea

ABSTRACT: Self-healing microfibers with core–shell geometry were studied. A commercial binary epoxy was encased in solution-blown polymer nano-/microfibers in the 0.2–2.6 μm diameter range. The core–shell microfibers were formed by coaxial nozzles, which encapsulated the epoxy resin and its hardener in separate cores. Solution blowing, the fiber-forming process used in this work, was at least 30 times faster than the electrospinning method used previously and has already been scaled up to the industrial level. These core–shell microfibers show self-healing capability, in which epoxy and hardener are released from the cores of damaged fibers, resulting in polymerization. The epoxy used had a higher strength and shorter solidification time than poly(dimethylsiloxane) (PDMS) used previously. Also, the larger fiber diameters in the present study facilitated faster release of the epoxy resin and its hardener from the fiber cores, shortening the solidification time in comparison to the previous studies. Blister tests were conducted, which measured the adhesion energy of microfiber mats to substrates and the cohesion energy between layers of microfiber mats before and after fatigue damage followed by self-healing.

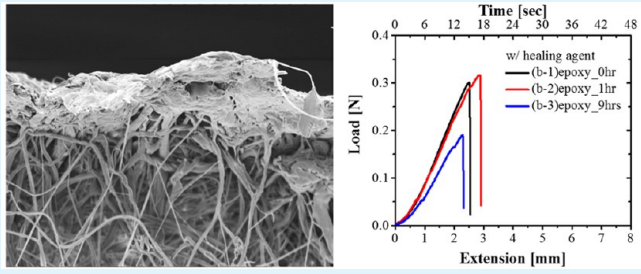

KEYWORDS: *self-healing, core–shell fibers, solution blowing, nano-/microfibers, adhesion*

1. INTRODUCTION

Self-healing processes are well-known to occur in nature (including in our own bodies), and efforts to incorporate similar properties in engineered materials have continued for at least the past decade. Catastrophic failures could happen in general constructions, public transport, and multiple other facilities, as well as prostheses subjected to fatigue caused by prolong periodic loading and/or corrosion. For example, a football-sized hole suddenly opened in an aircraft fuselage during a flight due to sudden crack propagation (Southwest Airlines flight, 2009).[1] Overall, damage accumulation resulting in catastrophic failures of this kind can affect multiple structures and materials, from military to home appliances, e.g., bridges, buildings, motor vehicles, aircrafts, and boats, etc., which can experience damage accumulation leading to crack propagation or delamination and where self-healing might be desirable. At the early stages of these studies, most of the efforts on polymers were aimed at dicyclopentadiene (DCPD) and Grubbs' catalyst.[2−5] When encapsulated DCPD in the material is released by a propagating crack and comes in contact with Grubbs' catalyst, also dispersed in the surrounding material, a polymerization reaction begins and the crack is, in principle, filled with newly formed polymer and is potentially healed. Poly(dimethylsiloxane) (PDMS) is also used as a healing agent because of the advantages in its mechanical and environmental properties.[6−8] The PDMS system is silicon-based, made up of two parts: a resin monomer and a curing agent. In engineered self-healing materials, these two components are kept separated in capsules embedded in the materials and are released when the capsules are ruptured. Polymerization then begins, and the newly formed PDMS polymer heals the damaged site. Recently, several other materials have been proposed as new healing agent candidates. These include, for example, supramolecular polymers, modified rubbers, and polymeric hydrogels, which restore and rejoin broken linkages by self-assembly.[9−14]

In most of the cases the healing agents are incorporated in the engineered materials in capsules or supplied through a vascular network. The single-usage capsules are not reused after they release the stored healing agent.[6−8] However, in the case of vascular networks (i.e., interconnected fibers or tubes) the healing agent can be supplied to the same spot several times for repeatable healing.[15−17] The bioinspired vascular systems can be adapted to the fiber-reinforced polymer (FRP) composites utilized in the aerospace and automotive industries.[18] In these applications, it is beneficial to reduce the lateral size of fiber-based vascular tubes to diminish their interference with the overall material structure. For this reason, electrospinning and solution blowing have been employed to form networks of core–shell nano- and microfibers filled with healing agents.[19−24] Both processes have been widely applied in the past decade[25−30] and are now established techniques, which are covered in detail in a recently published comprehensive monograph.[31]

In the previous studies, the healing agent (PDMS) was embedded in the cores of electrospun nanofibers.[32,33] In ref 22 two components of a potentially self-healing system, epoxide resin (bisphenol A–diglycidyl ether) and polyamine (polyetheramine), were dispersed separately, electrospun and

Received: December 17, 2015
Accepted: February 2, 2016
Published: February 2, 2016

DOI: 10.1021/acsami.5b12358
ACS Appl. Mater. Interfaces 2016, 8, 4955–4962

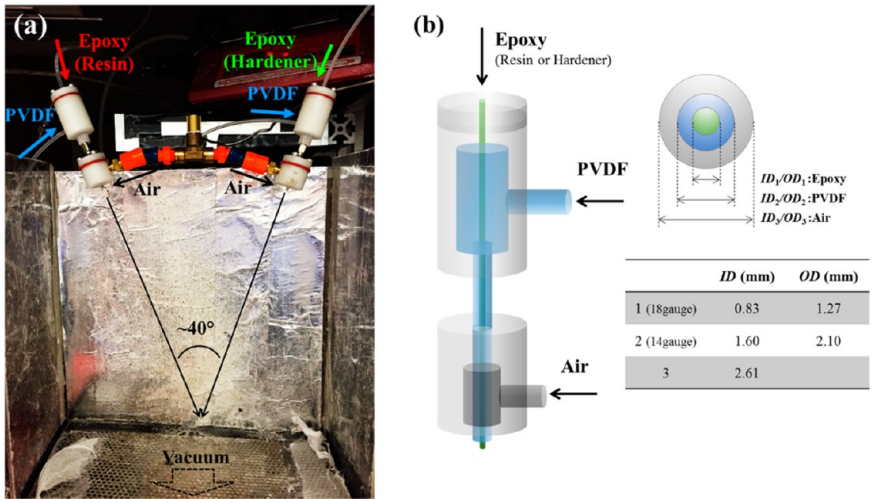

Figure 1. Solution blowing of core−shell nano- and microfibers: (a) experimental setup; (b) design of core−shell needle with coaxial air blowing nozzle. Epoxy- and hardener-cored fibers are produced simultaneously and uniformly mixed in the deposited fiber mat.

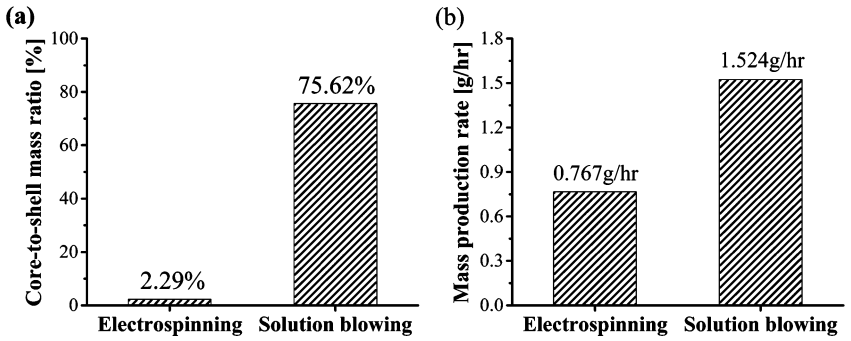

Figure 2. Comparison of the (a) core-to-shell mass ratio and (b) mass production rate for coaxial electrospinning and solution blowing of core−shell nano- and microfibers. The core and shell materials for electrospinning are PDMS resin and PAN.[38,39] The core and shell materials for solution blowing (present study) are epoxy resin and PVDF/PEO.

encased in fibers. Electrospinning of self-healing agents, catalyst and epoxy, was also conducted in ref 23. Liquid epoxy was confined in the core separated from the catalyst, which was encased in the surrounding shell, and both agents came in contact only after a fiber had been broken. As a fabrication technique, coaxial electrospinning is a simple and reliable way to encapsulate liquid agents inside continuous nano- and microfibers. From the material point of view, PDMS is one of the most attractive self-healing agents given its chemical, mechanical, optical, and biocompatibility properties. However, it takes 24−48 h for full curing and polymerization of PDMS at room temperature. Also, fully cured PDMS is relatively soft and flexible. Therefore, it is not suitable for the applications which require a relatively fast response (a shorter curing time) and a sufficient rigidity of the solidified material with relatively high strength and stiffness. Testing the resulting mechanical properties of cured materials is imperative and involves peeling, blistering, and dead-weight tests.[34−37]

In the present study, a commercial epoxy was employed for the first time as a healing agent embedded in nano- and microfibers that were formed using solution blowing. The epoxy begins hardening rapidly (in about 5 min) after activation and is fully cured in an hour. It provides the tensile strength up to 4400 psi (=30.33 MPa), as measured by direct pull-off of a test piece from a substrate. For the study of self-healing systems, the two components (resin monomer and hardener) were encapsulated separately in the cores of nano- and microfibers formed by solution blowing of poly(vinylidene difluoride) (PVDF) polymer using compressed air. After that, the self-healing properties of such nano- and microfiber mats were explored using the adhesion/delamination (blister) test accompanied by periodic bending fatigue. The aim of the present work is in the fast-response (5−60 min) novel self-healing materials for industrial applications, where they should be used to prevent delamination on ply surfaces, which are not exposed to environmental conditions.

2. EXPERIMENTAL SECTION

2.1. Materials and Solutions. For this study, PVDF ($M_w \approx 180$ kDa), PEO (poly(ethylene oxide); $M_w = 200$ kDa), DMF (*N*,*N*-dimethylformamide; anhydrous 99.8%), and acetone were purchased from Sigma-Aldrich. A PVDF solution for the shell material was prepared by mixing 5.0 g of PVDF solution (21 wt % in the acetone/DMF mixture, 2:3 (wt %)) and 2.0 g of PEO solution (4 wt % in the acetone/DMF mixture, 2:10 (wt %)). A two-part commercial epoxy kit (ClearWeld, produced by JB WELD) was purchased in a hardware store. According to its specifications, it has a 1:1 mixing ratio, sets in 5 min, and is fully cured in 1 h under ambient conditions. Both resin and hardener are nonvolatile materials. They were diluted with DMF (8:5 (wt %)) to lower their viscosities. According to notes on the Material Safety Data Sheet for this commercial epoxy, the resin is a reaction product of epichlorohydrin (C_3H_5ClO) and bisphenol-A ($C_{15}H_{16}O_2$; CAS No. 25085-99-8; 100%), while the hardener is predominantly polyalkoxylated hydroxyalkyl thiol (<75%).

DOI: 10.1021/acsami.5b12358
ACS Appl. Mater. Interfaces 2016, 8, 4955−4962

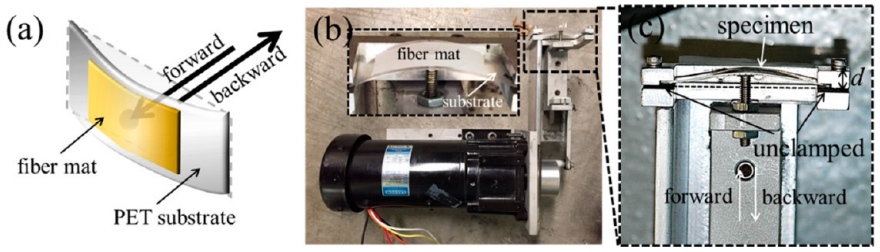

Figure 3. Bending for fiber mat fatigue: (a) schematic of specimen fatigue by bending; (b and c) details of the experimental setup.

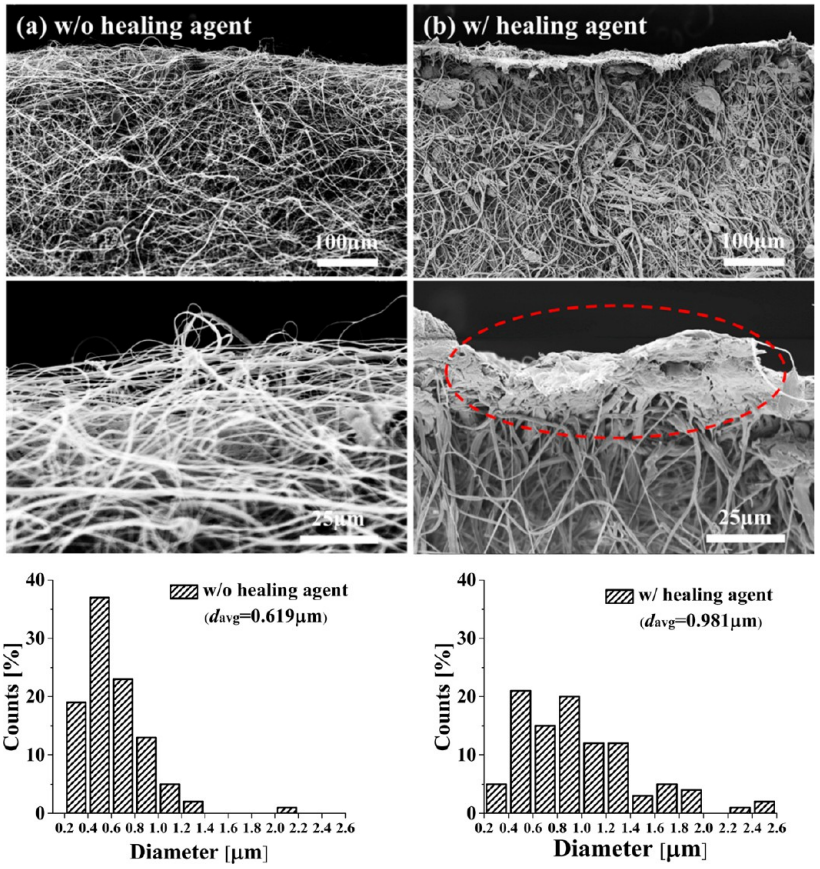

Figure 4. SEM images of cut fiber mats (the upper and middle images) and the corresponding fiber size distributions (the lower graphs): (column a) without healing agents and (column b) with healing agents in the fiber core.

2.2. Dual Coaxial Solution Blowing. The solution blowing setup used to form the self-healing core−shell nano- and microfibers and details of the core−shell needles and coaxial air nozzle used are shown in Figure 1. The core solution, containing either resin or hardener, and the shell solution (PVDF) were supplied separately to a core−shell needle with the flow rates of 5.0 mL/h for the core and 1.0 mL/h for the shell. Each core−shell needle was inserted into a coaxial air nozzle issuing pressurized air (40−50 psi). The resin and hardener-cored fibers were produced simultaneously in two separate core−shell needle setups (Figure 1). For a uniformly mixed deposition of the two types of fibers onto a permeable collector surface, the angle between the two needles was set to about 40° by an adjustable joint. The vacuum line installed under the permeable collector facilitates fiber adhesion to the collecting mesh. The air blowing conditions were optimized by controlling air pressure, needle-to-collector distance, and flow rate, etc. The solution-blown core−shell nano- and microfibers were collected for 10−20 min and then peeled from the collecting mesh. It should be emphasized that the amount of self-healing material introduced and the rate of forming of core−shell fibers using solution blowing are significantly higher than when using coaxial electrospinning, as shown in Figure 2. In fact, the core-to-shell mass ratio for solution blowing is 33 times higher than for electrospinning (75.62%/2.29%), while the total mass production rate is 2 times (1.524 g·h^{-1}/0.767 g·h^{-1}) higher.

In addition, for direct comparison of mass production rates of solution blowing and electrospinning, monolithic nanofibers were formed using the same material Nylon-6 solution (12 wt % in formic acid). The maximum flow rates for reliable fiber formation using solution blowing and electrospinning without dripping, with the other parameters (nozzle-to-substrate distance, applied voltage or air pressure, and nozzle diameter, etc.) being fixed, were respectively Q_{SB} = 5−10 mL/h and Q_{ES} = 0.1−0.3 mL/h. Also, in electrospinning the voltage was in the 6.5−13 kV range, the nozzle-to-substrate distance was 15 cm, and the nozzle (18G) with i.d./o.d. = 0.838 mm/1.270 mm. Accordingly, the ratio of the mass production rate of solution blowing to that of electrospinning was 33.3 (as 10 mL·h^{-1}/0.3 mL·h^{-1}).

2.3. Blister Test (Adhesion or Cohesion Tests). When the self-healing core−shell microfiber mats are damaged, the healing agents stored in the core are released and solidify as an adhesive. The adhesion energy was measured using a blister test. Thus, (i) the adhesion of the microfiber mat to a substrate, and (ii) the cohesion between the microfibers were characterized. The microfiber mats with

DOI: 10.1021/acsami.5b12358
ACS Appl. Mater. Interfaces 2016, 8, 4955−4962

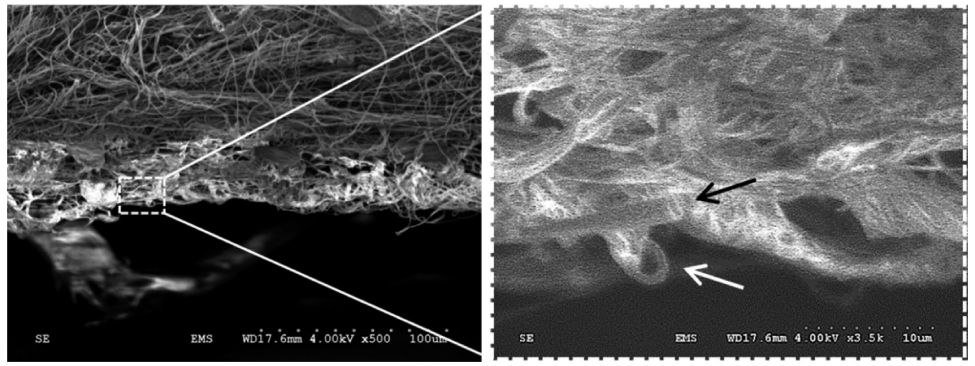

Figure 5. Frozen and broken fiber mat. In the right-hand image two arrows point at visible fiber cores.

and without a healing agent in the fiber cores were cut in pieces 20 × 30 mm^2 in size and placed on flexible polyethylene terephthalate (PET) substrates of thickness 0.73 mm. A steel roller (90 mm diameter) was rolled 10 times over a microfiber mat by hand, with sufficient pressure to facilitate adhesion to the substrate. Next, for the cohesion test, a sheet of microfibers was stuck to the substrate by dual-sided tape and another sheet of microfiber mat placed on top of the first one. A roller was then used to press both microfiber mats together to facilitate cohesion between them.

2.4. Sample Fatigue. To mimic damage caused by natural fatigue of the material, some specimens of core–shell microfiber mats were bent multiple times (cf. Figure 3) prior to the blister test. They were located on a PET substrate, which was repeatedly bent by a motor-driven shaft. A deflection amplitude d = 3 mm applied with frequency f = 1 Hz results in moderate bending fatigue of the unclamped flexible specimen. The damage accumulated during 1–9 h of bending can result in delamination of the fiber mat from the substrate [which would be revealed in the adhesion (blister) test] or a cohesive failure inside the fiber mat, as well as disintegration of some fibers.

3. RESULTS AND DISCUSSION

Each microfiber mat was cut with scissors; the cut edges are shown in Figure 4. The broken PVDF microfibers without

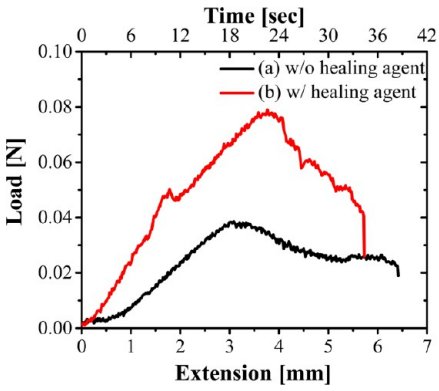

Figure 6. Load-extension curves in blister tests quantifying sample adhesion to the substrate. The samples were finger-pressed to the substrate.

stored epoxy in their core reveal a clear-cut edge as seen in Figure 4a. In comparison, the microfibers with healing agents in their core revealed accumulation of cured epoxy at the cut edge (see the red dashed circle in the middle part of Figure 4b). The average diameters of the fibers without and with healing agents stored in their cores were 0.619 and 0.981 μm, respectively. Note that in a separate experiment it was found that the average diameter of fibers with either resin or hardener was 1.563 or

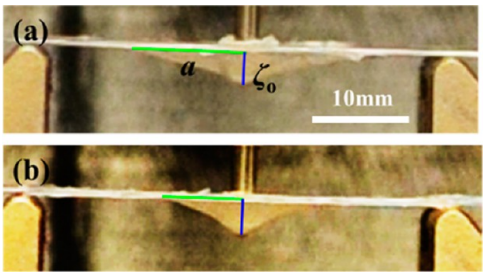

Figure 7. Photographic images of the blister test. The images correspond to blister tests of the fiber mats in the following cases: (a) without healing agents and (b) with healing agents in the fiber core.

Table 1. Adhesion Energy T and Data Corresponding to the Blister Tests, with ζ_o Being the Vertical Extension at Peak Loading[a]

	a (mm)	ζ_o (mm)	P (N)	h (mm)	E (MPa)	T (J/m^2)
a	11.52	3.28	0.039	0.11	2.725	0.067
b	8.24	3.56	0.079	0.12	2.125	0.307

[a]Other parameters are defined following eq 1. Rows a and b correspond to curves a and b in Figure 6. Note also that separate measurements revealed Young's moduli of fiber mats with either resin or hardener as 6.34 or 1.85 MPa, respectively.

0.675 μm, respectively. It should be emphasized that the resulting fiber diameters in solution blowing are controlled by the volumetric flow rates and the elongational viscosities of polymer solutions, the needle diameters, and the speed of air blowing.[31] The entrainment of the core material into the shell jet increases the outer diameter of the core–shell fibers compared to that of the fibers formed from a monolithic shell material.

To visualize the presence of the cores, a fiber mat with healing agents in the core was frozen by dipping in liquid nitrogen and then broken. Even though most of the cut fibers rapidly released resin, the SEM image on the right-hand side in Figure 5 reveals the fiber cores.

The adhesion energy between the fiber mat and substrate was found using the blister test. The test described in later text allows measurement of the blister shape and the pushing force that produces it. The physical model accounts for the elastic stretching of the relatively soft materials such as nano- and microfibers used in the present study. The theoretical background of the blister test and its data analysis are available in ref 38. Accordingly, the adhesion energy is found as

DOI: 10.1021/acsami.5b12358
ACS Appl. Mater. Interfaces 2016, 8, 4955–4962

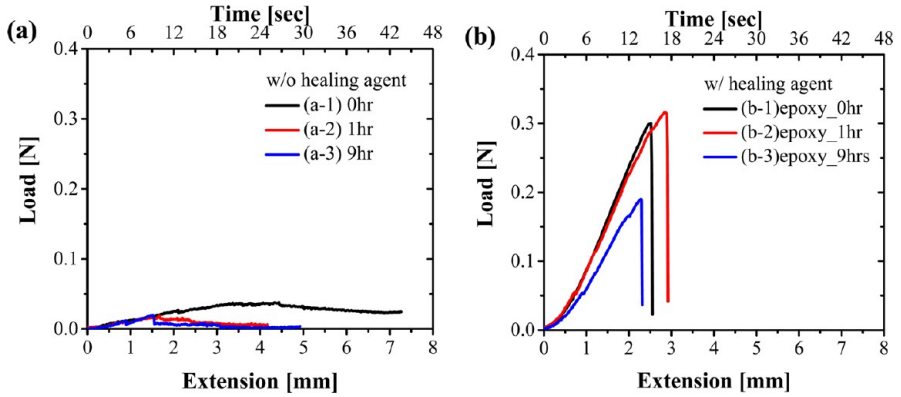

Figure 8. Load-extension curves in blister tests quantifying sample adhesion to the substrate: (a) without epoxy precursors and (b) with epoxy precursors in the fiber cores. All samples were initially roller-pressed to the substrate. Curves marked as (-1) correspond to pristine (unfatigued) samples, curves marked as (-2) correspond to samples after 1 h of fatigue, and curves marked as (-3) correspond to samples after 9 h of fatigue.

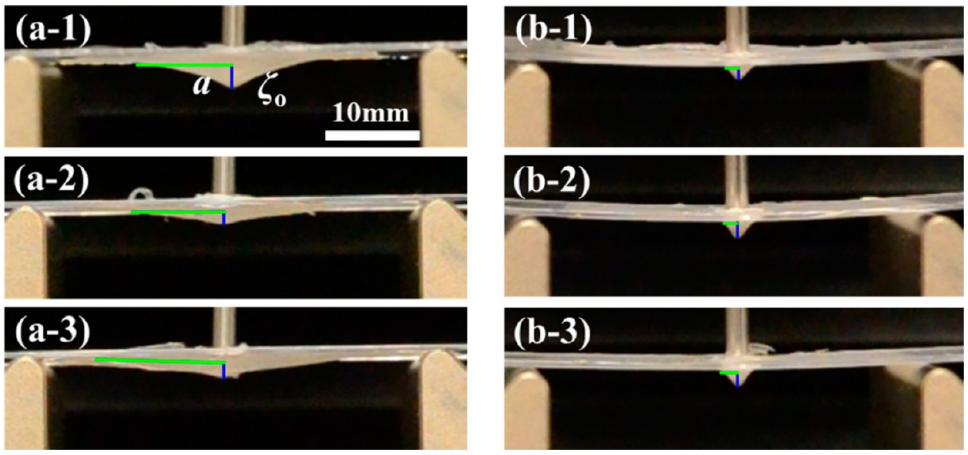

Figure 9. Photographic images of blister tests of samples (a-1−a-3) without epoxy precursors and (b-1−b-3) with epoxy precursors in the fiber cores. All samples were initially roller-pressed to the substrate. Fatigue levels (1−3) are as designated in Figure 8.

Table 2. Adhesion energy T and All Parameters Measured in the Blister Tests[a]

	a (mm)	ζ_o (mm)	P (N)	h (mm)	E (MPa)	T (J/m^2)
a-1	10.31	3.63	0.037	0.09	2.725	0.071
a-2	10.06	1.65	0.018			0.028
a-3	13.81	1.52	0.019			0.021
b-1	1.63	2.52	0.300	0.08	2.125	15.354
b-2	1.69	2.87	0.316			15.575
b-3	2.06	2.28	0.189			3.735

[a]Rows a-1−a-3 and b-1−b-3 correspond to the curves in Figure 8 and are for samples without and with epoxy precursors in the fiber cores, respectively.

$$T = \frac{3}{8}\left(\frac{1}{\pi^4 Eh}\right)^{1/3}\left(\frac{P}{a}\right)^{4/3} \quad (1)$$

where T is the adhesion energy, E is Young's modulus, h is the thickness of the fiber mat, P is the peak load, and a is the radius of the blistered area at peak loading. The Young's moduli E of the fiber mats were measured using a tensile test at a strain rate of 10 mm/min.

The adhesion tests of fiber samples placed on a PET substrate were conducted to confirm that the healing agents (the epoxy precursors) were encased in the fiber cores and to demonstrate the healing effect. For control, monolithic PVDF fibers were formed without a core enclosing healing agents and also used in the blister tests. In these tests, the fiber mats without and with epoxy in the cores were placed onto a flexible PET substrate and then pressed by finger. The adhesion energy associated with detachment of these fiber mats from the substrate was measured by using the blister test.[39] The adhesion energy T found from the data (cf. Figures 6 and 7) using eq 1 yields the values of $T = 0.307$ J/m^2 (see Table 1) for the samples containing the epoxy precursors in the fiber cores and $T = 0.067$ J/m^2 for the samples without epoxy. The 5-fold increase in the adhesion energy in the former case results from the epoxy precursors in the cores being released upon pressing the fibers and, thus, bonding them to the substrate. This confirms the presence of the epoxy precursors in the fiber cores and their release under pressure or bending.

For a more controlled method of adhering fiber samples to the substrate, a metal roller was passed over the fiber mat samples on the substrate 10 times. Figures 8 and 9, associated with these rolled samples, reveal that the blister size and the load-extension dependence are significantly affected by epoxy precursors in the fiber cores. We also note that adhesion of the fiber samples without epoxy precursors deteriorates dramatically due to fatigue. Specifically, after 1 h of bending fatigue (a-2), the adhesion energy T drops to about 40% of that in the pristine case (a-1; cf. Table 2). For a longer duration of the bending test (9 h; a-3) the adhesion energy is identical to that

DOI: 10.1021/acsami.5b12358
ACS Appl. Mater. Interfaces 2016, 8, 4955−4962

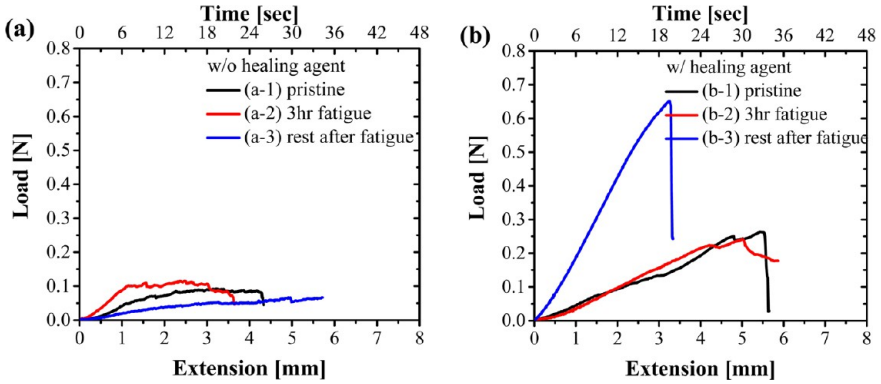

Figure 10. Load-extension curves to quantify cohesion between fiber mats: (a) without precursors and (b) with epoxy precursors in the fiber cores. Samples were roller-pressed. Curves marked as (-1) correspond to pristine samples, (-2) indicates samples after 3 h of fatigue and tested almost immediately, and (-3) indicates samples after 3 h of fatigue and 24 h of rest before the blister test.

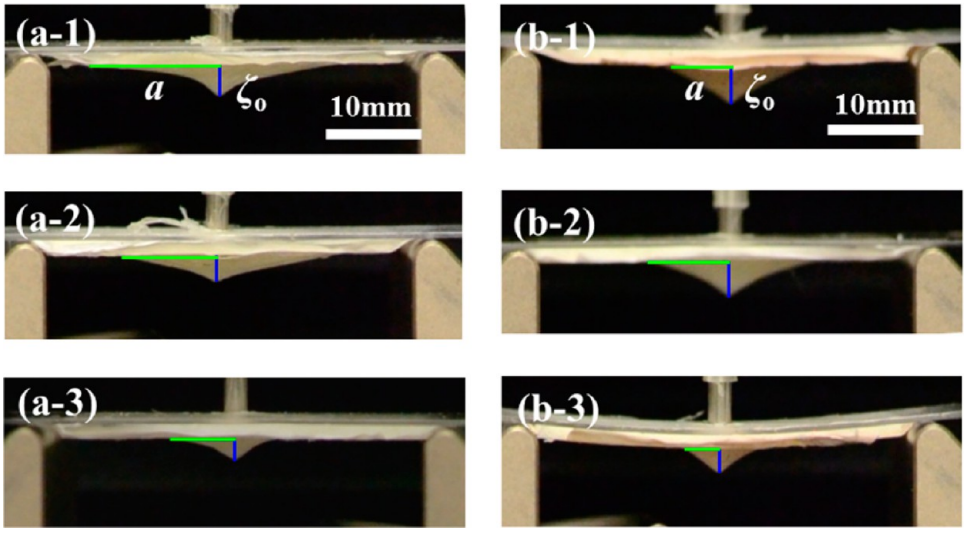

Figure 11. Photographic images of blister tests of samples (a-1−a-3) without epoxy precursors and (b-1−b-3) with epoxy precursors in the fiber cores. All samples were initially roller-pressed to the substrate. Fatigue levels (1−3) are as designated in Figure 10.

Table 3. Cohesion Energy *T* and All Parameters Measured in the Blister Test[a]

	a (mm)	ζ_o (mm)	*P* (N)	*h* (mm)	*E* (MPa)	*T* (J/m^2)
a-1	13.73	4.17	0.087	0.09	2.725	0.153
a-2	10.13	3.00	0.106			0.298
a-3	6.86	4.97	0.067			0.127
b-1	6.54	5.47	0.263	0.08	2.125	2.004
b-2	8.63	5.02	0.242			1.987
b-3	3.73	3.25	0.651			16.385

[a]Rows a-1−a-3 and b-1−b-3 correspond to the curves in Figure 10, indicating fibers without and with epoxy precursors in their cores.

measured after 1 h, showing that the main damage to the fiber mat and its adhesion to the substrate occurred in this case during the first hour.

For the samples with epoxy precursors in the fiber cores, the adhesion energy of the pristine sample (b-1) is much higher than that of the pristine samples lacking the epoxy precursors in the core (a-1). This result (with roller-pressing used) is similar to that with finger-pressing (cf. Figure 6). However, for the samples with epoxy precursors in the fiber cores, the adhesion energy remains unchanged after 1 h of bending (b-2) and drops to about 25% of the initial value after 9 h (b-3). The blister tests were conducted within several minutes of completion of either the 1 or 9 h of bending. It should be emphasized that the epoxy

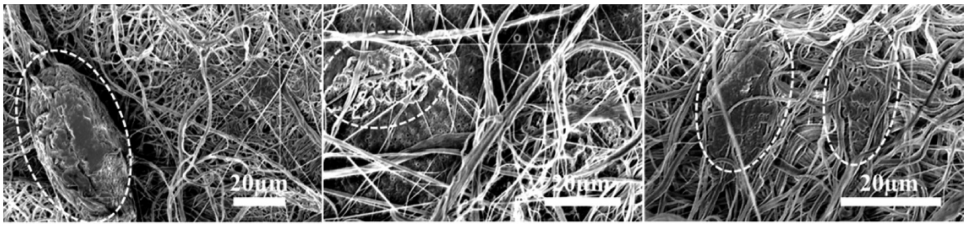

Figure 12. Resin and cure squeezed from the core−shell fibers after they underwent a prolong fatigue, blister test, and subsequent pressing.

DOI: 10.1021/acsami.5b12358
ACS Appl. Mater. Interfaces 2016, 8, 4955−4962

used sets in 5 min, which is comparable to the time between the bending fatigue and blister tests, which is thus sufficient for curing of the damaged self-healing samples. The adhesion between the substrate and the fiber mat may have recovered after 1 h of fatigue by self-healing, as the results in Figure 8b show, although it is not clear whether sufficient sample damage was caused by 1 h of fatigue to validate this conclusion. However, the data in Figure 8b show that the sample did not fully recover by self-healing from 9 h of fatigue.

Next, for the cohesion experiments (i.e., the adhesion at the interface between two fiber mats instead of the adhesion between a fiber mat and the substrate), a layer of fiber mat was attached to the substrate using dual-sided tape, another layer of a similar fiber mat was placed on it, and the fiber mat layers were pressed against each other with the roller. A blister test was then used to measure the cohesion energy, i.e., the energy required for delamination of the upper fiber layer from the bottom layer. The results and the experiments are shown in Figures 10 and 11. The corresponding cohesion energies T listed in Table 3 reveal that, for the fiber mat without epoxy precursors, the measured cohesion energies are relatively close for all three cases: for the pristine sample (a-1), for the sample tested after 3 h of bending (a-2), and for the sample tested after 3 h of bending followed by 24 h of rest time (a-3). However, for the self-healing samples containing epoxy precursors in the fiber cores, the pattern is different. For the pristine sample (b-1) and the sample tested after 3 h fatigue (b-2) the cohesion energies are close, while, for the sample tested after 3 h followed by the 24 h rest time (b-3), it is increased by 8 times. This is associated with the fact that the epoxy precursors released from the fiber cores during the fatigue test have sufficient time to react and solidify, a process that not only heals the damaged interface but significantly reinforces it.

It should be emphasized that the self-healing fiber mats contained a significant amount of resin and cured even after prolonged damage (fatigue) and the subsequent blister test, which is demonstrated in Figure 12, where they were squeezed from the fibers after pressing.

Note, also, that similar nanofiber mats studied in ref 38 revealed self-healing in tensile tests even after the fourth cycle of fatigue.

4. CONCLUSION

Solution blowing allows one to form core−shell fiber mats with epoxy precursors (epoxy resin or its hardener stored separately in the fiber cores) more efficiently than electrospinning [the core-to-shell mass ratio is 33 times higher (75.62%/2.29%), and the total mass production rate is 2 times higher (1.524 $g{\cdot}h^{-1}$/0.767 $g{\cdot}h^{-1}$); the mass production rate of monolithic nanofibers in solution blowing is 33.3 times higher than in electrospinning]. After being subjected to fatigue, these fibers revealed self-healing capabilities. In particular, the epoxy precursors were released from the cores of damaged fibers and reinforced the adhesion of the fiber mat to the substrate or cohesion between fiber mat layers. Blister tests were used to measure the adhesion and cohesion energies. In particular, an 8-fold increase in the cohesion energy was observed after 3 h of fatigue bending followed by a 24 h period of rest.

AUTHOR INFORMATION

Corresponding Authors

*(A.L.Y.) E-mail: ayarin@uic.edu.

*(S.S.Y.) E-mail: skyoon@korea.ac.kr.

Notes

The authors declare no competing financial interest.

ACKNOWLEDGMENTS

This work was supported by the International Collaboration Program funded by the Agency for Defense Development.

REFERENCES

(1) Goldsmith, S. Southwest Airlines Flight 2294 Lands in West Virginia with Football-Sized Hole in Fuselage. http://www.nydailynews.com/news/world/southwest-airlines-flight-2294-lands-west-virginia-football-sized-hole-fuselage-article-1.397715.

(2) White, S. R.; Sottos, N. R.; Geubelle, P. H.; Moore, J. S.; Kessler, M. R.; Sriram, S. R.; Brown, E. N.; Viswanathan, S. Autonomic Healing of Polymer Composites. *Nature* **2001**, *409*, 794−797.

(3) Kessler, M. R.; Sottos, N. R.; White, S. R. Self-Healing Structural Composite Materials. *Composites, Part A* **2003**, *34*, 743−753.

(4) Brown, E. N.; White, S. R.; Sottos, N. R. Retardation and Repair of Fatigue Cracks in a Microcapsule Toughened Epoxy Composite − Part I: Manual Infiltration. *Compos. Sci. Technol.* **2005**, *65*, 2466−2473.

(5) Brown, E. N.; White, S. R.; Sottos, N. R. Retardation and Repair of Fatigue Cracks in a Microcapsule Toughened Epoxy Composite—Part II: In Situ Self-Healing. *Compos. Sci. Technol.* **2005**, *65*, 2474−2480.

(6) Cho, S. H.; Andersson, H. M.; White, S. R.; Sottos, N. R.; Braun, P. V. Polydimethylsiloxane-Based Self-Healing Materials. *Adv. Mater.* **2006**, *18*, 997−1000.

(7) Keller, M. W.; White, S. R.; Sottos, N. R. A Self-Healing Poly(Dimethyl Siloxane) Elastomer. *Adv. Funct. Mater.* **2007**, *17*, 2399−2404.

(8) Cho, S. H.; White, S. R.; Braun, P. V. Self-Healing Polymer Coatings. *Adv. Mater.* **2009**, *21*, 645−649.

(9) Cordier, P.; Tournilhac, F.; Soulie-Ziakovic, C.; Leibler, L. Self-Healing and Thermoreversible Rubber from Supramolecular Assembly. *Nature* **2008**, *451*, 977−980.

(10) Burnworth, M.; Tang, L.; Kumpfer, J. R.; Duncan, A. J.; Beyer, F. L.; Fiore, G. L.; Rowan, S. J.; Weder, C. Optically Healable Supramolecular Polymers. *Nature* **2011**, *472*, 334−338.

(11) Burattini, S.; Colquhoun, H. M.; Fox, J. D.; Friedmann, D.; Greenland, B. W.; Harris, P. J. F.; Hayes, W.; Mackay, M. E.; Rowan, S. J. A Self-Repairing, Supramolecular Polymer System: Healability as a Consequence of Donor−Acceptor Π−Π Stacking Interactions. *Chem. Commun.* **2009**, No. 44, 6717−6719.

(12) Sordo, F.; Mougnier, S.-J.; Loureiro, N.; Tournilhac, F.; Michaud, V. Design of Self-Healing Supramolecular Rubbers with a Tunable Number of Chemical Cross-Links. *Macromolecules* **2015**, *48*, 4394−4402.

(13) Jia, Y.-G.; Zhu, X. X. Self-Healing Supramolecular Hydrogel Made of Polymers Bearing Cholic Acid and B-Cyclodextrin Pendants. *Chem. Mater.* **2015**, *27*, 387−393.

(14) Das, A.; Sallat, A.; Bohme, F.; Suckow, M.; Basu, D.; Wießner, S.; Stockelhuber, K. W.; Voit, B.; Heinrich, G. Ionic Modification Turns Commercial Rubber into a Self-Healing Material. *ACS Appl. Mater. Interfaces* **2015**, *7*, 20623−20630.

(15) Toohey, K. S.; Hansen, C. J.; Lewis, J. A.; White, S. R.; Sottos, N. R. Delivery of Two-Part Self-Healing Chemistry Via Microvascular Networks. *Adv. Funct. Mater.* **2009**, *19*, 1399−1405.

(16) Toohey, K. S.; Sottos, N. R.; Lewis, J. A.; Moore, J. S.; White, S. R. Self-Healing Materials with Microvascular Networks. *Nat. Mater.* **2007**, *6*, 581−585.

(17) Patrick, J. F.; Hart, K. R.; Krull, B. P.; Diesendruck, C. E.; Moore, J. S.; White, S. R.; Sottos, N. R. Continuous Self-Healing Life Cycle in Vascularized Structural Composites. *Adv. Mater.* **2014**, *26*, 4302−4308.

(18) Coope, T. S.; Wass, D. F.; Trask, R. S.; Bond, I. P. Metal Triflates as Catalytic Curing Agents in Self-Healing Fibre Reinforced Polymer Composite Materials. *Macromol. Mater. Eng.* **2014**, *299*, 208−218.

DOI: 10.1021/acsami.5b12358
ACS Appl. Mater. Interfaces 2016, 8, 4955−4962

(19) Sinha-Ray, S.; Pelot, D. D.; Zhou, Z. P.; Rahman, A.; Wu, X.-F.; Yarin, A. L. Encapsulation of Self-Healing Materials by Coelectrospinning, Emulsion Electrospinning, Solution Blowing and Intercalation. *J. Mater. Chem.* **2012**, *22*, 9138−9146.
(20) Wu, X.-F.; Rahman, A.; Zhou, Z.; Pelot, D. D.; Sinha-Ray, S.; Chen, B.; Payne, S.; Yarin, A. L. Electrospinning Core-Shell Nanofibers for Interfacial Toughening and Self-Healing of Carbon-Fiber/Epoxy Composites. *J. Appl. Polym. Sci.* **2013**, *129*, 1383−1393.
(21) An, S.; Liou, M.; Song, K. Y.; Jo, H. S.; Lee, M. W.; Al-Deyab, S. S.; Yarin, A. L.; Yoon, S. S. Highly Flexible Transparent Self-Healing Composite Based on Electrospun Core-Shell Nanofibers Produced by Coaxial Electrospinning for Anti-Corrosion and Electrical Insulation. *Nanoscale* **2015**, *7*, 17778−17785.
(22) Park, J.-H.; Braun, P. V. Coaxial Electrospinning of Self-Healing Coatings. *Adv. Mater.* **2010**, *22*, 496−499.
(23) Bijlard, A.-C.; Kaltbeitzel, A.; Avlasevich, Y.; Crespy, D.; Hamm, M.; Landfester, K.; Taden, A. Dual-Compartment Nanofibres: Separation of Two Highly Reactive Components in Close Vicinity. *RSC Adv.* **2015**, *5*, 97477−97484.
(24) Zanjani, J. S. M.; Okan, B. S.; Letofsky-Papst, I.; Menceloglu, Y.; Yildiz, M. Repeated Self-Healing of Nano and Micro Scale Cracks in Epoxy Based Composites by Tri-Axial Electrospun Fibers Including Different Healing Agents. *RSC Adv.* **2015**, *5*, 73133−73145.
(25) Reneker, D. H.; Yarin, A. L.; Fong, H.; Koombhongse, S. Bending Instability of Electrically Charged Liquid Jets of Polymer Solutions in Electrospinning. *J. Appl. Phys.* **2000**, *87*, 4531−4547.
(26) Zussman, E. Encapsulation of Cells within Electrospun Fibers. *Polym. Adv. Technol.* **2011**, *22*, 366−371.
(27) Sun, Z.; Zussman, E.; Yarin, A. L.; Wendorff, J. H.; Greiner, A. Compound Core-Shell Polymer Nanofibers by Co-Electrospinning. *Adv. Mater.* **2003**, *15* (22), 1929−1932.
(28) Zussman, E.; Chen, X.; Ding, W.; Calabri, L.; Dikin, D. A.; Quintana, J. P.; Ruoff, R. Mechanical and Structural Characterization of Electrospun Pan-Derived Carbon Nanofibers. *Carbon* **2005**, *43*, 2175−2185.
(29) Shi, L.; Zhuang, X.; Tao, X.; Cheng, B.; Kang, W. Solution Blowing Nylon 6 Nanofiber Mats for Air Filtration. *Fibers Polym.* **2013**, *14*, 1485−1490.
(30) Zhuang, X.; Yang, X.; Shi, L.; Cheng, B.; Guan, K.; Kang, W. Solution Blowing of Submicron-Scale Cellulose Fibers. *Carbohydr. Polym.* **2012**, *90*, 982−987.
(31) Yarin, A. L.; Pourdeyhimi, B.; Ramakrishna, S. *Fundamentals and Applications of Micro- and Nanofibers*; Cambridge University Press: Cambridge, U.K., 2014.
(32) Lee, M. W.; An, S.; Lee, C.; Liou, M.; Yarin, A. L.; Yoon, S. S. Self-Healing Transparent Core-Shell Nanofiber Coatings for Anti-Corrosive Protection. *J. Mater. Chem. A* **2014**, *2*, 7045−7053.
(33) Lee, M. W.; An, S.; Lee, C.; Liou, M.; Yarin, A. L.; Yoon, S. S. Hybrid Self-Healing Matrix Using Core−Shell Nanofibers and Capsuleless Microdroplets. *ACS Appl. Mater. Interfaces* **2014**, *6*, 10461−10468.
(34) Hu, S.; Xia, Z.; Gao, X. Strong Adhesion and Friction Coupling in Hierarchical Carbon Nanotube Arrays for Dry Adhesive Applications. *ACS Appl. Mater. Interfaces* **2012**, *4*, 1972−1980.
(35) Cao, Z.; Wang, P.; Gao, W.; Tao, L.; Suk, J. W.; Ruoff, R. S.; Akinwande, D.; Huang, R.; Liechti, K. M. A Blister Test for Interfacial Adhesion of Large-Scale Transferred Graphene. *Carbon* **2014**, *69*, 390−400.
(36) Wang, W. J.; Liu, T. F.; Wang, H. Y.; Liu, Q. Y.; Zhu, M. H.; Jin, X. S. Influence of Friction Modifiers on Improving Adhesion and Surface Damage of Wheel/Rail under Low Adhesion Conditions. *Tribol. Int.* **2014**, *75*, 16−23.
(37) Sett, S.; Lee, M. W.; Weith, M.; Pourdeyhimi, B.; Yarin, A. L. Biodegradable and Biocompatible Soy Protein/Polymer/Adhesive Sticky Nano-Textured Interfacial Membranes for Prevention of Esca Fungi Invasion into Pruning Cuts and Wounds of Vines. *J. Mater. Chem. B* **2015**, *3*, 2147−2162.
(38) Lee, M. W.; An, S.; Jo, H. S.; Yoon, S. S.; Yarin, A. L. Self-Healing Nanofiber-Reinforced Polymer Composites: 1. Tensile Testing and Recovery of Mechanical Properties. *ACS Appl. Mater. Interfaces* **2015**, *7*, 19546−19554.
(39) Lee, M. W.; An, S.; Jo, H. S.; Yoon, S. S.; Yarin, A. L. Self-Healing Nanofiber-Reinforced Polymer Composites: 2. Delamination/Debonding, and Adhesive and Cohesive Properties. *ACS Appl. Mater. Interfaces* **2015**, *7*, 19555−19561.

DOI: 10.1021/acsami.5b12358
ACS Appl. Mater. Interfaces 2016, 8, 4955−4962